Article

Mononuclear Fe(I) and Fe(II) Acetylene Adducts and their Reductive Protonation to Terminal Fe(IV) and Fe(V) Carbynes

Cooper Citek, Paul H. Oyala, and Jonas C. Peters

J. Am. Chem. Soc., **Just Accepted Manuscript** • DOI: 10.1021/jacs.9b06987 • Publication Date (Web): 20 Aug 2019

Mononuclear Fe(I) and Fe(II) Acetylene Adducts and their Reductive Protonation to Terminal Fe(IV) and Fe(V) Carbynes

Cooper Citek, Paul H. Oyala, and Jonas C. Peters*

Division of Chemistry and Chemical Engineering, California Institute of Technology, Pasadena, California 91125, United States

ABSTRACT: The activity of nitrogenase enzymes, which catalyze the conversion of atmospheric dinitrogen to bioavailable ammonia, is most commonly assayed by the reduction of acetylene gas to ethylene. Despite the practical importance of acetylene as a substrate, little is known concerning its binding or activation in the iron-rich active site. "Fischer-Tropsch" type coupling of non-native C_1 substrates to higher-order $C_{\geq 2}$ products is also known for nitrogenase, though potential metal-carbon multiply-bonded intermediates remain underexplored. Here we report the activation of acetylene gas at a mononuclear tris(phosphino)silyl-iron center, $(SiP_3)Fe$, to give Fe(I) and Fe(II) side-on adducts, including S =1/2 $Fe^{I}(\eta^2\text{-HCCH})$; the latter is characterized by pulse EPR spectroscopy and DFT calculatoins. Reductive protonation reactions with these compounds converge at stable examples of unusual, formally iron(IV) and iron(V) carbyne complexes, as in diamagnetic $(SiP_3)Fe{\equiv}CCH_3$ and the paramagnetic cation S = 1/2 $[(SiP_3)Fe{\equiv}CCH_3]^+$. Both alkylcarbyne compounds possess short Fe-C triple bonds (approx. 1.7 Å) trans to the anchoring silane. Pulse EPR experiments, X-band ENDOR and HYSCORE, reveal delocalization of the iron-based spin onto the α-carbyne nucleus in carbon p-orbitals. Furthermore, isotropic coupling of the distal β-CH_3 protons with iron indicates hyperconjugation with the spin/hole character on the $Fe{\equiv}C\text{-}CH_3$ unit. The electronic structures of $(SiP_3)Fe{\equiv}CCH_3$ and $[(SiP_3)Fe{\equiv}CCH_3]^+$ are discussed in comparison to previously characterized, but hetero-substituted, iron carbynes, and also a hypothetical nitride species, $(SiP_3)Fe{\equiv}N$. Such comparisons are germane to the consideration of formally high-valent, multiply-bonded Fe≡C and/or Fe≡N intermediates in synthetic or biological catalysis by iron.

INTRODUCTION

Interest in nominally high valent iron nitrides (N^{3-}) and imides (NR^{2-}) has grown in the past 15-20 years,[1] and has stemmed from a desire to explore their electronic structures and reactivity patterns, especially as they may pertain to important synthetic and biological transformations. For instance, the intermediacy of an Fe≡N species has been considered in the context of a distal pathway for biological nitrogen fixation by nitrogenase enzymes ($Fe\text{-}N_2 + 3\ H^+/e^- \rightarrow Fe{\equiv}N + NH_3$).[2] Relatedly, such an intermediate nitride has been recently characterized within a synthetic iron system that catalyzes N_2-to-NH_3 conversion.[3]

Nitrogenase enzymes reduce a range of non-native substrates as well, including for example azide (N^{3-}), cyanide (CN^-), CO, CO_2, and acetylene (C_2H_2).[4] Indeed, acetylene reduction to ethylene (C_2H_4) is the most convenient and hence most common assay for reductive "nitrogenase" activity.[5,6,7] It is perhaps surprising, therefore, that acetylene complexes of iron, and their associated reactivity patterns, have not been well-studied to date. Noting this gap, we undertook a study of the reactivity of acetylene with an iron system supported by a tripodal phosphine ligand, in part for comparison with related studies we and others had undertaken in the context of N_2 chemistry. As a result, we uncovered an unexpectedly rich reactivity profile that links acetylene binding at iron(I) to the ultimate generation of nominally high-valent (+4 and +5) iron carbynes via reductive protonation steps. While these transformations do not appear to model the reactivity profile of acetylene reduction by nitrogenase, they are nevertheless fascinating.

Until recently, iron carbynes of any type had little synthetic precedent.[8,9,10,11,12] Reductive activation of CO and CN^- at iron recently led to examples of heteroatom-substituted (i.e., Fischer-type) iron carbynes.[10,11] By contrast, the alkylcarbynes featured herein ($Fe^{IV}{\equiv}CCH_3$ and $[Fe^{V}{\equiv}CCH_3]^+$) are unique in that they are not substituted by heteroatoms. In a broader context, iron complexes featuring strong iron-to-carbon multiple bonds are of continuing interest, especially as they may pertain to intermediates in "Fischer-Tropsch" type C-C coupling pathways exhibited by nitrogenase enzymes in the presence of non-native CO, CO_2, and CN^- substrates.[4]

Herein, we describe the following:

(i) The first complexes featuring C_2H_2 bound to a single iron center are characterized, in the formal +1 and +2 oxidation states (i.e., $Fe^{I}(C_2H_2)$ and $Fe^{II}(C_2H_2)^+$); the iron(I) derivative is S = ½, and pulse EPR data confirm η_2 side-on coordination.

(ii) Well-characterized examples of $Fe^{IV}{\equiv}CCH_3$ and $Fe^{V}{\equiv}CCH_3^+$ carbynes are presented, including their solid-state X-ray crystal structures and ^{57}Fe Mössbauer spectra. The $Fe^{V}{\equiv}CCH_3^+$ species is S = ½ and pulse EPR spectroscopy is used to additionally map its electronic structure.

(iii) Mechanistic studies indicate the $Fe^{I}(C_2H_2)$ species undergoes initial C-H activation, followed by bimolecular H_2 loss, to generate a terminal $Fe^{II}C{\equiv}CH$, which can also be independently prepared. The $Fe^{V}{\equiv}CCH_3^+$ species is most conveniently accessed by reductive protonation steps from $Fe^{II}C{\equiv}CH$.

The EPR data provided for $Fe^{I}(C_2H_2)$ and $Fe^{V}{\equiv}CCH_3^{+}$ could be of value to mechanistic studies employing related EPR techniques of nitrogenases with C_2H_2,[13] or to studies of non-native C_1 substrates that lead to Fischer-Tropsch type C-C couplings.[4]

RESULTS AND DISCUSSION

Mononuclear iron-acetylene adducts

Figure 1 outlines the entire reaction manifold discussed herein, where a tris(phosphino)silyl-iron subunit (abbreviated herein as "$(SiP_3)Fe$" or "Fe") is common to all of the complexes described. To test the affinity of acetylene for an iron(I) center, the previously reported complex $(SiP_3)Fe^{I}N_2$ (**1**) was exposed to acetylene gas. Displacement of N_2 by 1.2 equivalents of acetylene occurs slowly at room temperature in THF to give an unobserved acetylene adduct complex, $(SiP_3)Fe^{I}(\eta^2\text{-HCCH})$ **2** (see below for further characterization at low T), that proceeds to the red, terminal acetylide complex $(SiP_3)Fe^{II}CCH$ **3**, along with liberation of 0.5 equivalents of H_2 (confirmed by GC).

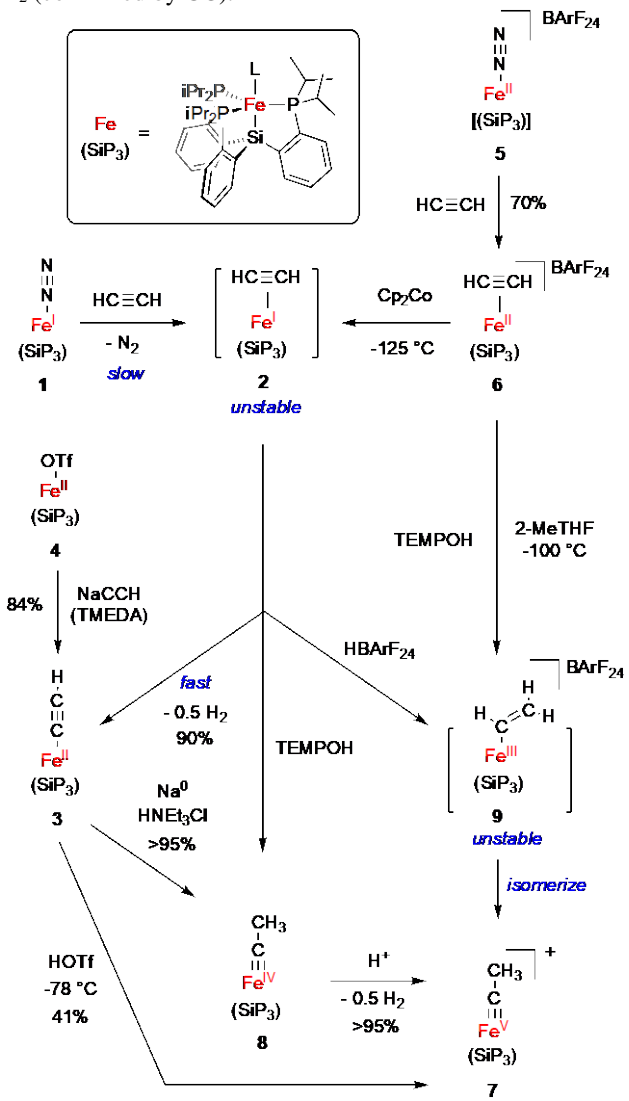

Figure 1. Scheme depicting the reaction chemistry discussed herein, along with labeled formal oxidation states and compound numbers.

The acetylide complex **3** can alternatively be prepared by stirring a sodium acetylide slurry with $(SiP_3)Fe^{II}OTf$ (**4**) in the presence of tetramethyl ethylenediamine (TMEDA) in 84% yield. The complex has been characterized in solution and the solid state (see Figure 2) as a trigonal bipyramidal $S = 1$ iron(II) species featuring the SiP_3 ligand. Complex **3** exhibits a weak C≡C vibration (1902 cm^{-1}) and a terminal C-H stretch (3277 cm^{-1}); isotopic labeling with $^{13}C_2$-TMED-LiC≡CH (see SI for preparation details) gives $^{13}C_2$**-2** ($\nu_{C\equiv C}$ = 1832 cm^{-1} and $\nu_{C\text{-}H}$ = 3262 cm^{-1}; $\Delta_{C\equiv C}$ = 70 cm^{-1}; $\Delta_{C\text{-}H}$ = 15 cm^{-1}; Figure S23). Three other terminal iron-acetylide compounds have previously been crystallographically characterized.[14]

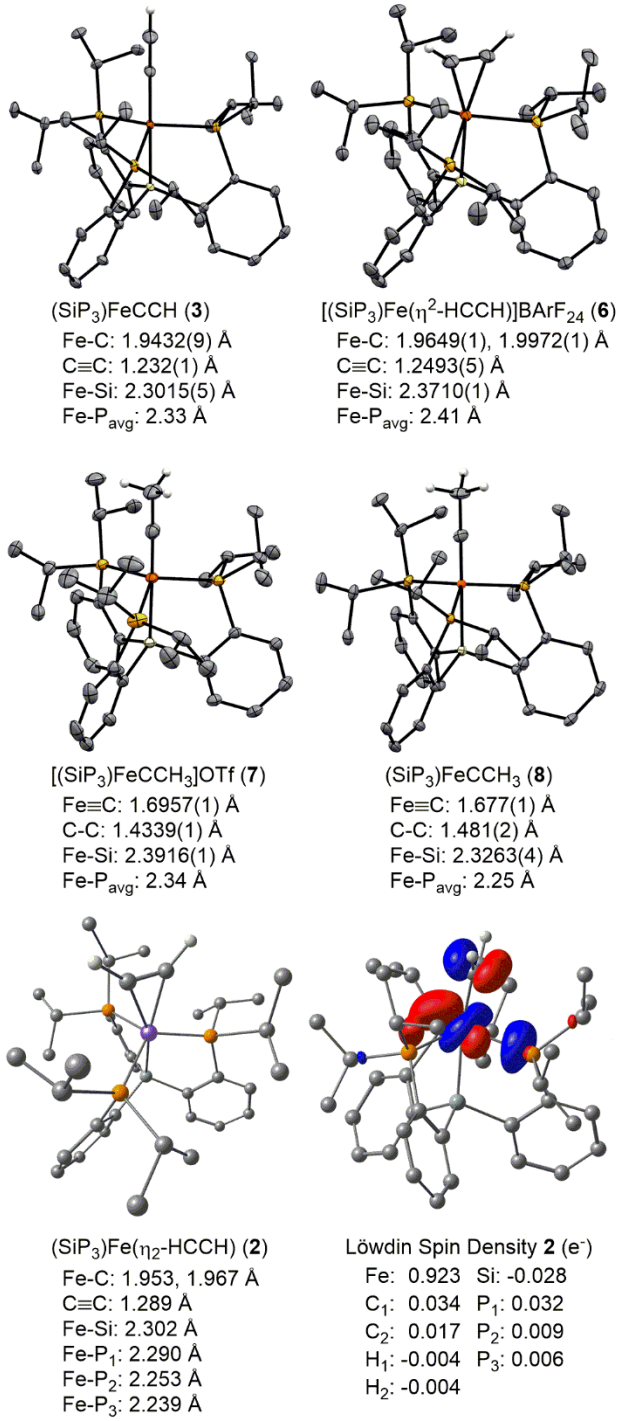

Figure 2. Solid-state crystal structures of **3**, **6**, **7**, and **8**, with thermal ellipsoids displayed at 50% probability. The hydrogen atoms of (SiP_3) and the counter-anions present in the structures for **6** and **7** have been omitted for clarity. A DFT-minimized structure of $(SiP_3)Fe^{I}(\eta^2\text{-}C_2H_2)$ **2** is also shown, with bond metrics, along with the calculated SOMO orbital and Löwdin spin densities in the primary ligation sphere.

A thermally stable adduct of acetylene is accessible at the iron(II) state. Accordingly, the light-blue cation $[(SiP_3)FeN_2]BArF_{24}$ (**5**)[15] ($BArF_{24}$ = $[B(3\text{-}5\text{-}(CF_3)_2\text{-}C_6H_3)_4]^-$) reacts with one equivalent of acetylene gas in fluorobenzene at 0 °C to afford green $[(SiP_3)Fe(\eta^2\text{-}HCCH)]BArF_{24}$ (**6**) (70% isolated yield). The solid-state X-ray structure of the S = 1 complex shows the η^2-HCCH ligand bound side-on in the axial position opposite to the silyl anchor (Figure 2). As stated in the introduction, complex **6** is to our knowledge the only example (other than **2**, *vide infra*) of a mononuclear iron complex featuring C_2H_2 as a ligand.[16] Mononuclear adducts of acetylene are highly uncommon for first row metals in general.[17] Fe-to-acetylene backbonding in **6** is modest (C≡C bond length of 1.25 Å; cf. 1.20 Å in free acetylene[18]) and the Fe-P and Fe-Si bond are relatively long, in accord with its S = 1 ground state and side-on accommodation of the acetylene ligand.

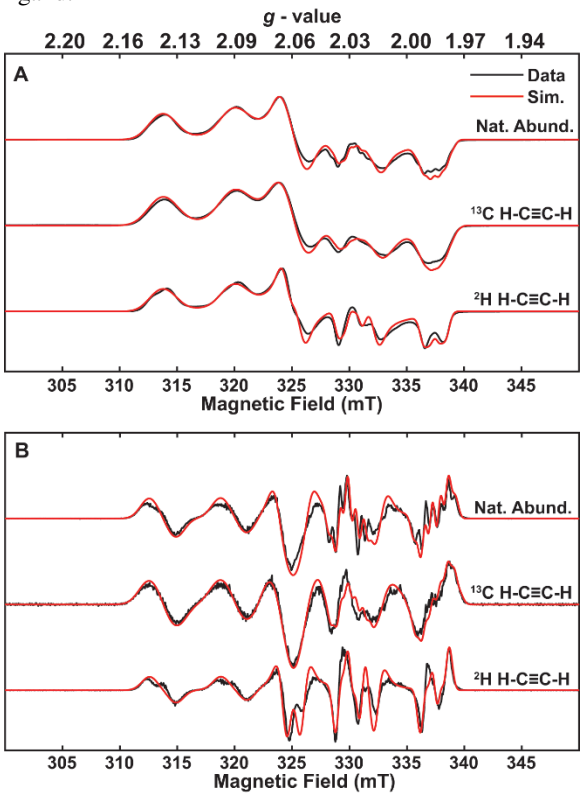

Figure 3. (a) X-band CW-EPR spectra of $(SiP_3)Fe(\eta^2\text{-}HCCH)$ prepared in 2-MeTHF with natural abundance (top), ^{13}C-enriched (middle), and ^{2}H-enriched acetylene (bottom) with simulations using parameters in Table 1 overlaid in red. (b) Derivative spectra of X-band CW-EPR for each isotopologue with simulations overlaid in red. Acquisition parameters: temperature = 77 K; MW frequency = 9.375 GHz; MW power = 2 mW; modulation frequency = 100 kHz; modulation amplitude = 0.1 mT; conversion time = 41 ms.

Because the acetylene adduct $Fe^I(\eta^2\text{-}HCCH)$ **2** cannot be observed upon addition of C_2H_2 to Fe^IN_2 **1** at room temperature (owing to slow ligand substitution kinetics), we sought its characterization via the low temperature reduction of $[Fe^{II}(\eta^2\text{-}HCCH)]^+$ **6**. Thus, addition of stoichiometric cobaltocene (Cp_2Co) to a stirred solution of **6** in 2-MeTHF at -125 °C rapidly generates a new orange species that exhibits first order decay above -80 °C to generate the terminal acetylide $Fe^{II}CCH$ **3** ($t_{1/2}$(-40°C) ≈ 14 min; monitored by *in situ* UV-visible spectroscopy; Figure S54).

To more thoroughly characterize $Fe^I(\eta^2\text{-}HCCH)$ **2**, in particular to assess whether alternative "$Fe^{III}(CCH_2)$" or "$Fe^{III}(H)(CCH)$" isomers might be more appropriate, we undertook continuous wave (CW) and pulse EPR experiments of both the natural abundance and deuteron-labeled isotopologue $Fe^I(\eta^2\text{-}DCCD)$ at X-band frequency, coupled with DFT studies. The X-band CW EPR spectrum, shown in Figure 3a,b, exhibits a g-tensor with rhombic symmetry (g = [2.114, 2.040, 2.007]) with coupling evident to three distinct phosphorous nuclei. Simulation of the data indicates that one of the P-donors is coupled more strongly than the other two ($|A(^{31}P)|$ = [183, 182, 214] MHz, Table 1). These simulated coupling values, and especially the asymmetry with respect to one donor, qualitatively agree with the DFT-predicted ^{31}P hyperfine tensors calculated from an optimized structure of **2** ($|A(^{31}P)|$ = [201, 203, 242] MHz; TPSS/def2-TZVP/D3ZERO; see SI for details).

Complementary X-band Electron Nuclear Double Resonance (ENDOR) and Hyperfine Sublevel Correlation (HYSCORE) spectroscopic data allow for further resolution of the coupling of the paramagnetic iron center with NMR active nuclei. Accordingly, hyperfine coupling of the acetylene ^{1}H nuclei to the spin on iron can be extracted by comparison of the data for $Fe^I(\eta^2\text{-}HCCH)$ with that for $Fe^I(\eta^2\text{-}DCCD)$. Field-dependent HYSCORE (Figure 4) and ^{1}H-^{2}H ENDOR (Figure 5) spectra show weak ^{1}H hyperfine couplings to two very similar acetylene-derived protons: $^1H_1$ ($|A(^1H)|$ = [9.4, 20.2, 17.6] MHz, with Euler rotation angles [α,β,γ] = [33, 18, -5] relative to the g-tensor and $^1H_2$($|A(^1H)|$ = [8.2, 18.4, 16.8] MHz, with Euler rotation angles [α,β,γ] = [43, -22, 11]. These results are also corroborated by the appearance of ^{2}H features in the HYSCORE data for $Fe^I(\eta^2\text{-}DCCD)$, which are well simulated by scaling these hyperfine tensors by the ratio of the ^{1}H/^{2}H gyromagnetic ratios (γ^1H/γ^2H = 6.514) (Figures S33-35). These two protons exhibit extremely similar isotropic hyperfine couplings, with $a_{iso}(^1H_1)$ = 15.7 MHz and $a_{iso}(^1H_2)$ = 14.5 MHz, and are only differentiated by the respective orientations of their hyperfine tensors relative to the molecular g-tensor coordinate frame, which is resolved in the ^{1}H-^{2}H difference ENDOR data acquired near the low-field edge of the EPR spectrum (see Figure 5, top trace). This observation strongly disfavors assignment as the "$Fe^{III}(H)(CCH)$" isomer, as a hydride directly bound to an S = 1/2 iron center should exhibit much stronger coupling (a_{iso} ≈ 45 MHz).[19,20]

To distinguish between the $Fe^I(\eta^2\text{-}HCCH)$ and "$FeCCH_2$" isomers, we prepared the ^{13}C-enriched derivative $^{13}C_2H_2$-**2**. Consistent fits between the field-dependent ^{13}C-^{12}C difference HYSCORE (Figure 6) and ENDOR spectra (See SI) give two nearly identical, strongly coupled ^{13}C nuclei $^{13}C_1$($|A(^{13}C)|$ = [17, 24, 8.6], a_{iso} = 16.5 MHz; $^{13}C_2$($|A(^{13}C)|$ = [24, 16.6, 10.2] a_{iso} = 16.9 MHz) (Table 1), which also disfavors the "$FeCCH_2$" isomer, as such a species would be anticipated to show highly inequivalent $^{13}C_\alpha$ and $^{13}C_\beta$ couplings, with coupling to C_α being much larger. Together, these EPR data are fully consistent with a structure for **2** formulated as an η^2-HCCH adduct of iron(I), akin to its one-electron oxidized derivative **6**.

Table 1. Hyperfine coupling constants in MHz determined for $(SiP_3)Fe(\eta^2\text{-}HCCH)$

Nucleus	A_1	A_2	A_3	a_{iso}	Euler angles [α,β,γ]°
$^{31}P_1$	183	183	214	193.3	[0, 0, 0]
$^{31}P_2$	30	28	40	32.7	[0, 0, 0]
$^{31}P_3$	12	0.5	17	9.8	[0, 0, 0]
$^1H_1$	9.4	20.2	17.6	15.7	[33, 18, -5]
$^1H_2$	8.2	18.4	16.8	14.5	[43, -22, 11]

$^{13}C_1$	17	24	8.6	16.5	[0, 30, 0]
$^{13}C_2$	24	16.6	10.2	16.9	[0, -30, 0]

Several other side-on adducts of alkynes and alkenes at reduced Fe(I) centers have been reported by Holland and coworkers.[21] These complexes exhibit high-spin S = 3/2 ground state electronic structures and were described with substantial π-backbonding from iron to the coordinated unsaturated ligand. In a study of an α-70^{Val} mutant nitrogenase that is able to accommodate several substituted-acetylene substrates, the S = 3/2 resting state EPR signal is, by contrast, converted to an iron-localized rhombic S = 1/2 doublet in a freeze-quenched experiment using propargyl alcohol (HC≡CCH$_2$OH) as the substrate.[13] This doublet signal closely matches that of a CO-bound/inhibited state. While ^{13}C coupling to the doublet signal was measured, it was not possible to distinguish between possible binding modes of the propargyl alcohol.

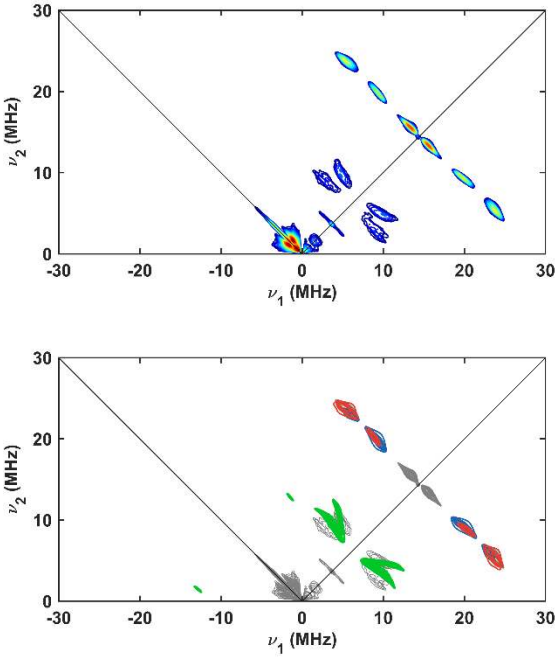

Figure 4. (top) X-band HYSCORE spectrum of natural abundance (SiP$_3$)Fe(η^2-HCCH) acquired at 338.6 mT (g = 2.058). (bottom) Monochromatic representation of the HYSCORE data with simulations using parameters in Table 1 overlaid: (red) ^{1}H-1 (blue) ^{1}H-2, (green) ^{31}P-3. Acquisition parameters: temperature = 20 K; microwave frequency = 9.751 GHz; MW pulse length (π/2, π) = 8 ns, 16 ns; τ = 138 ns, $t_1 = t_2$ = 100 ns; $\Delta t_1 = \Delta t_2$ = 16 ns; shot repetition time (srt) = 1 ms).

The transformation of Fe^I(η^2-HCCH) **2** to acetylide Fe^{II}CCH **3** is interesting to consider further. The available data is insufficient to determine the fate of **2** after its first-order decay. However, two distinct paths seem most plausible to us. In one scenario, which we favor, C-H oxidative addition of the coordinated C_2H_2 ligand produces "Fe^{III}(H)(CCH)", one of the structural isomers considered above. This intermediate then loses half an equivalent of H_2 in a bimolecular step. Relatedly, we recently reported an example of bimolecular H_2 loss from a well-defined Fe^{III}-hydride complex that features a sufficiently weak Fe-H bond.[20] Additionally, the oxidative addition pathway (Figure 7) is well precedented for a number of previously characterized alkyne-hydride complexes of Co and Fe.[22] Of note to the present study, we previously reported reversible activation of phenylacetylene in a structurally related trisphosphine-borane TPBFe system, likely by oxidative addition to a formally Fe(II)-alkyne-hydride/borohydride complex.[23]

Alternatively, another reaction pathway could involve eventual rearrangement of Fe^I(η^2-HCCH) **2** or an intermediate Fe^{III}(H)(CCH) to the end-on "FeCCH$_2$" isomer, considered above, again followed by bimolecular H_2 loss. However, transformation by a *unimolecular* 1,2 hydrogen shift of an η^2-alkyne adduct to a terminal alkylidene/vinylidene[24] is generally thought to have a high barrier and is therefore difficult without an exogenous acid/base catalysts or high temperature.[25] Berke and coworkers have reported that chromatography on silylated silica accelerates the formation of terminally stable vinylidene complexes from mixtures of low-valent iron acetylene/alkyne and alkyene-hydride complexes.[22c,26] In the present Fe^I(η^2-HCCH) **2** system, deprotonation by solvent (THF) to produce [FeCCH]$^-$, followed by re-protonation to produce FeCCH$_2$, seems highly unlikely considering the low acidity expected for **2** in THF. Finally, while we consider it to be unlikely, a bimolecular reaction between Fe^I(η^2-HCCH) and itself, or with Fe^{III}(H)(CCH), could in principle evolve H_2.

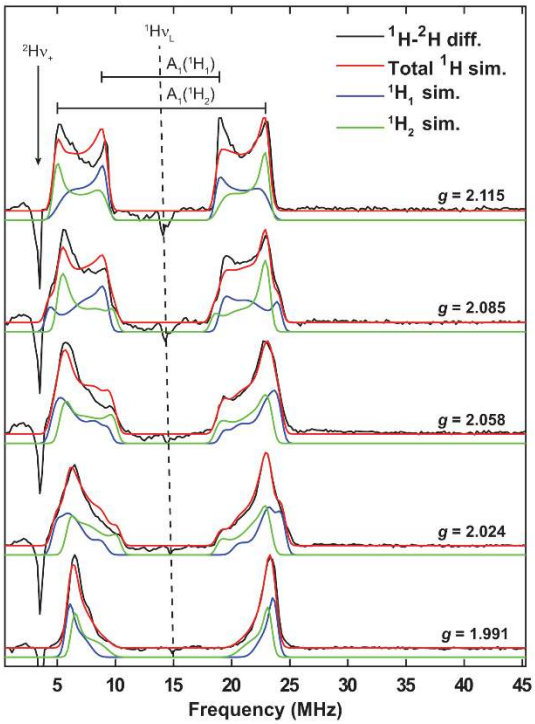

Figure 5. Field-dependent X-band ^{1}H-minus-^{2}H Davies ENDOR difference spectra of (SiP$_3$)Fe(η^2-HCCH) (black) with simulations using parameters in Table 1 overlaid: (red) total ^{1}H simulation, (blue) ^{1}H-1, (green) ^{1}H-2. Acquisition parameters: temperature = 15 K; MW frequency = 9.751 GHz; MW pulse length (π/2, π) = 40 ns, 80 ns; τ = 260 ns; RF pulse length = 15 μs; T_{RF} = 2 μs; shot repetition time = 5 ms.

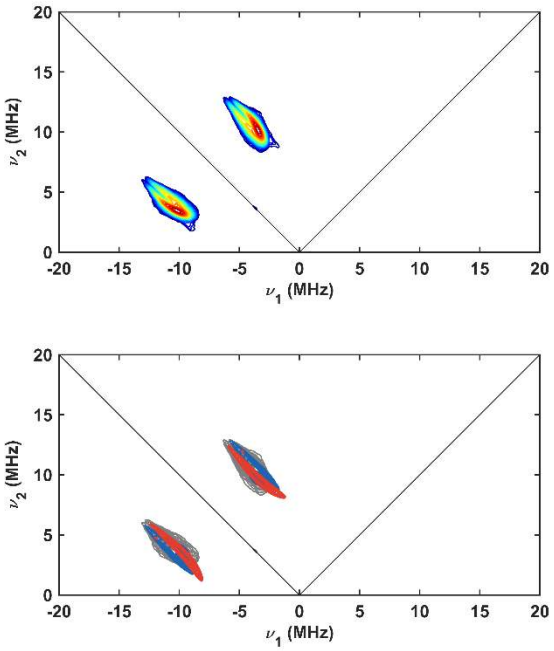

Figure 6. (top) X-band ^{13}C-^{12}C difference HYSCORE spectrum of $(SiP_3)Fe(\eta^2\text{-}HCCH)$ acquired at 338.6 mT (g = 2.058). (bottom) Monochromatic representation of the HYSCORE data with ^{13}C simulations using parameters in Table 1 overlaid: (blue) $^{13}C_1$, (red) $^{13}C_2$. Acquisition parameters: temperature = 20 K; microwave frequency = 9.751 GHz; MW pulse length ($\pi/2$, π) = 8 ns, 16 ns; τ = 138 ns, $t_1 = t_2$ = 100 ns; $\Delta t_1 = \Delta t_2$ = 16 ns; shot repetition time (srt) = 1 ms).

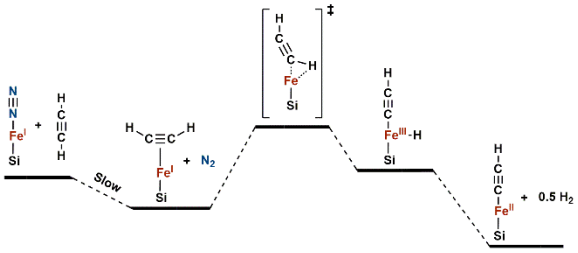

Figure 7. A qualitative reaction coordinate for the proposed slow substitution of acetylene for N_2 at $(SiP_3)FeN_2$, **1**, leading to intermediate $(SiP_3)Fe(\eta^2\text{-}HCCH)$ **2**, which subsequently undergoes sp(C-H)-activation and H_2 release to generate isolable $(SiP_3)Fe(CCH)$, **3**. We presume the H_2 elimination step occurs in a bimolecular fashion via two Fe(III)-hydride species. See text for a discussion of other possible pathways.

Terminal iron-carbyne complexes

The addition of triflic acid (HOTf) to the terminal Fe-acetylide **3** in diethyl ether at -78°C precipitates $[(SiP_3)Fe{\equiv}CCH_3][OTf]$ (**7**) as a dark brown solid from solution (40% yield). Use of $[H(Et_2O)_2][BArF_{24}]$ in place of HOTf affords $[(SiP_3)Fe{\equiv}CCH_3][BArF_{24}]$ (Figure 1). The alkylcarbyne cation **7** is a nominally iron(V) complex that, to our knowledge, is the only species of its type, formal or otherwise. The complex exhibits an S = 1/2 ground state (vide infra) and is stable as a solid or in THF or acetonitrile solution at room temperature for extended periods. As stated above, there are a handful of previously characterized, terminal, heteroatom-substituted carbynes of iron.[8,9,10,11,12] There are no prior examples of alkylcarbynes of iron, nor examples where the carbyne is substituted instead by H or aryl for that matter. Additionally, paramagnetic examples of carbyne/alkylidyne complexes are rare,[27,28] and, for first row metals, the only others we know of relate to $[(SiP_3)FeCNH_2]^+$ and $[(SiP_3)FeCNMe_2]^+$.[11,12]

The solid-state crystal structure of **7** is shown in Figure 2. As required for an S = 1/2 system, the complex deviates slightly from three-fold symmetry (∠P-Fe-P angles 114, 117, 120°). Most noteworthy is a characteristically short *Fe*≡*C*-CH_3 bond of 1.70 Å and a Fe≡*C*-*C*H_3 single bond of 1.42 Å. The Fe-Si bond is long at 2.39 Å, consistent with its position *trans* to the carbyne ligand. The triflate counter-anion exhibits close contacts with the (SiP_3)-isopropyl and carbyne C-H positions.

The conversion of $(SiP_3)FeCCH$ to $[(SiP_3)FeCCH_3]^+$ is a net 2-H^+/1-e^- transformation, requiring sacrificial oxidation of half of the starting iron material, for a theoretical 50% yield. Analysis of recovered material shows primarily $(SiP_3)FeOTf$ **4**, indicating the net reducing equivalent is likely derived from the acetylide moiety. The propensity for reaction intermediates to cannibalize themselves en route to **7** is consistent with the observed thermodynamic stability of the terminal product.

It is also noted that protonation of **3** by HOTf does not instead lead to its net oxidation (i.e., to form $(SiP_3)FeCCH^+$) with concomitant loss of 0.5 equivalents of H_2 (eq. 1), especially as the cationic $[(SiP_3)FeCCH]^+$ is electrochemically accessible (-0.78 V vs Fc in THF; Figure S58).[29]

$$FeCCH + HOTf \rightarrow [FeCCH]^+ + 0.5\ H_2 \quad \text{eq. 1}$$
(*not observed*)

Alternatively, protonation of acetylide **3** in ether by the weaker, insoluble acid, imidazolium triflate, to our surprise generates the neutral alkyl carbyne derivative, $(SiP_3)Fe{\equiv}CCH_3$ **8** (25% isolated yield), the product of a net 2 H^+ / 2 e^- reduction, again requiring some amount of sacrificial oxidation of starting material. The neutral carbyne **8** is thus more favorably synthesized in a heterogeneous mixture of triethylammonium chloride and excess sodium metal to balance the proton-coupled reduction (Figure 1). The $Fe{\equiv}CCH_3^+/Fe{\equiv}CCH_3$ redox couple between **7** and **8** occurs at -1.00 V vs Fc in THF (Figure S59); chemical oxidation of **8** by ferrocenium (Cp_2Fe^+) or a strong acid, like $[H(Et_2O)][BArF_{24}]$, cleanly generates **7**.

Carbyne **8** is diamagnetic with resolved coupling by ^1H, ^{31}P, and ^{13}C NMR spectroscopy (Figures S10-16). Isotopic labelling in **$^{13}C_2$-8** reveals a very downfield ^{13}C resonance for C_α at 348 ppm[30,31] with coupling to C_β (48 ppm; $J_{C(\alpha)\text{-}C(\beta)}$ = 18 Hz) and three equivalent phosphines (^{31}P 107.5 ppm; $J_{C(\alpha)\text{-}P}$ = 18 Hz). By ^1H NMR spectroscopy, the terminal carbyne C*H*$_3$ resonance at 2.12 ppm couples to C_α (11 Hz) and C_β (127 Hz). The primary ligation of **8** is contracted with respect to S = ½ $[Fe{\equiv}CCH_3]^+$ **7**, with a Fe≡C bond of 1.68 Å, a 2.33 Å Fe-Si bond, and Fe-P bonds between 2.24-2.26 Å (Figure 2), presumably consistent with increased backbonding upon reduction.

$(SiP_3)Fe{\equiv}CCH_3$ **8** is quite stable, even in solution at 130°C over a 24 hour time period. Its stability renders it a reaction sink in this system. Indeed, with its diagnostic NMR resonances in hand, it can be identified as a minor side-product of other reactions we have surveyed, including the aforementioned reaction between $(SiP_3)FeOTf$ and excess sodium acetylide (Figure 1).

The terminal stability of both alkylidyne complexes inspired us to further explore their interconnection with the acetylene complexes, described above, by reductive protonation reactions (Figure 1). Interestingly, net hydrogen atom transfer (HAT) reactions can convert the acetylene

adducts **2** and **6** to the carbynes **7** and **8**. For example, mixing $[Fe(\eta^2\text{-HCCH})]^+$ **6** with TEMPO-H in 2-MeTHF generates $Fe{\equiv}CCH_3^+$ **7**. At -100 °C, a relatively stable orange intermediate **9** can be observed by UV-visible spectroscopy, which then decays to **7** on warming (Figure S55). Our tentative assignment of **9** as a cationic alkenyl complex $[(SiP_3)Fe(CH{=}CH_2)]^+$, if correct, would make it a structurally interesting one. Whereas there is precedent for related, substituted iron alkenyl derivatives,[22g] the Fe-CH=CH_2 subunit is still, to our knowledge, distinct.

Cationic carbyne **7** can also be generated by the addition of stoichiometric $[H(Et_2O)_2][BArF_{24}]$ to a 2-MeTHF solution of $(SiP_3)Fe(\eta^2\text{-HCCH})$ **2** at -125 °C, presumably via **9** as an intermediate (Figure 1). Under similar conditions, the reaction of **2** with TEMPO-H generates the neutral carbyne **8**, along with $(SiP_3)FeCCH$ **2** as side product. There thus appears to be a rich reactivity landscape connecting the nascent acetylene adducts and terminal carbynes described herein.

Electronic structure of iron-carbyne complexes

The Mössbauer parameters for carbynes **7** and **8** compare well with those of the previously reported and structurally characterized iron carbynes featuring the same $(SiP_3)Fe$ subunit: $(SiP_3)Fe(COSiMe_3)$ and $[(SiP_3)Fe(CNMe_2)]^{0/+}$ (Table 2). The isomer shifts are relatively close to 0 mm s^{-1} across the series, reflecting strong covalency in the short Fe-C triple bond, with $Fe{\equiv}CCH_3^+$ **7** and and $Fe{\equiv}CCH_3$ **8** having the smallest δ values.[2b,3,32,33,34] By comparison, $[(SiP_3)FeCNMe_2]^+$ has an isomer shift of 0.19 mm s^{-1}, indicating less Fe≡C covalency, possibly consistent with a $[Fe{=}C{=}NMe_2]^+$ resonance form and its slightly longer *Fe-C* bond (1.74 Å). The measured quadrupole splittings for this series of carbynes are rather narrow, especially by comparison to the very large ΔE_Q values reported for other formally high-valent oxide and nitride Fe complexes in C_3 symmetry.[1k,2,3,33,34] Frontier orbital manifolds whereby the electrons populate only orbitals of d(xy) and $d(x^2\text{-}y^2)$ parentage, as for the d^4 and d^3 configurations described for the latter systems, is predicted to give large quadrupole splittings, > 5 mm s^{-1}, due to the strongly asymmetric, equatorially disposed electric field gradient at Fe.[32] By contrast, the comparatively small ΔE_Q values observed for the $(SiP_3)Fe$-carbyne series reflects the additional presence of substantial electron density along the z-axis (parallel to the *Fe≡C*-R vector). Inspection of the molecular orbitals of the carbyne series shows that the nominally high-lying Fe-C σ*-antibonding orbital is highly stabilized by mixing with Si(σ),[35] resulting in a heavily mixed orbital of a_1 symmetry energetically below the filled, primarily nonbonding orbitals of d(xy) and $d(x^2\text{-}y^2)$ parentage (Figure 8). This observation bears relevance to a contributing resonance structure we have previously considered, with electron density being polarized between a cationic R_3Si^+ anchor and a nominally reduced Fe center (Figure 9).[9,36]

Table 2. Mössbauer parameters of $(SiP_3)Fe$ carbynes

Fe≡CX	$OSiMe_3$[d]	NMe_2[e]	NMe_2^+[e]	CH_3	CH_3^+
Fe≡C[a]	1.67	1.71	1.74	1.68	1.70
Fe-Si[a]	2.30	2.31	2.35	2.33	2.39
δ[b]	0.061	0.058	0.19	-0.029	0.0097
ΔE_Q[b]	1.12	1.12	1.51	0.72	1.33
$^{13}C_\alpha$[c]	250.3	279.6	--	348.4	--

[a]approx. measurements in Å. [b]measured in mm s^{-1}. [c]measured in ppm in C_6D_6. [d]ref. 9. [e]ref. 10.

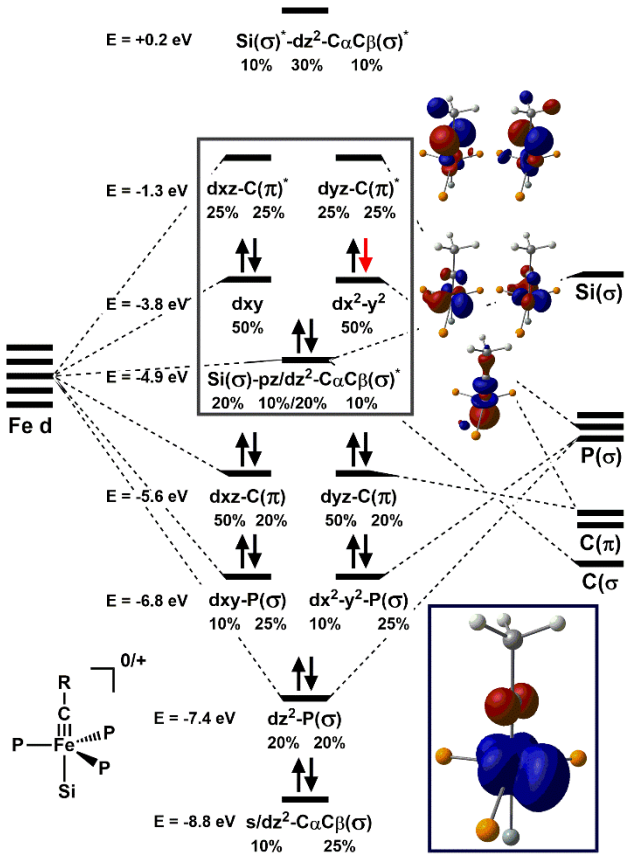

Figure 8. Simplified molecular orbital diagram for the metal-ligand bonding of a $(SiP_3)Fe{\equiv}CR$ carbyne in C_{3v} symmetry. Approximate orbital energies and compositions shown for $(SiP_3)FeCCH_3$ (TPSS/Def2-TZVP/D3ZERO). (Inset) DFT-predicted spin density map for $[(SiP_3)FeCCH_3]^+$ (isovalue: 0.005 e⁻/Å^3).

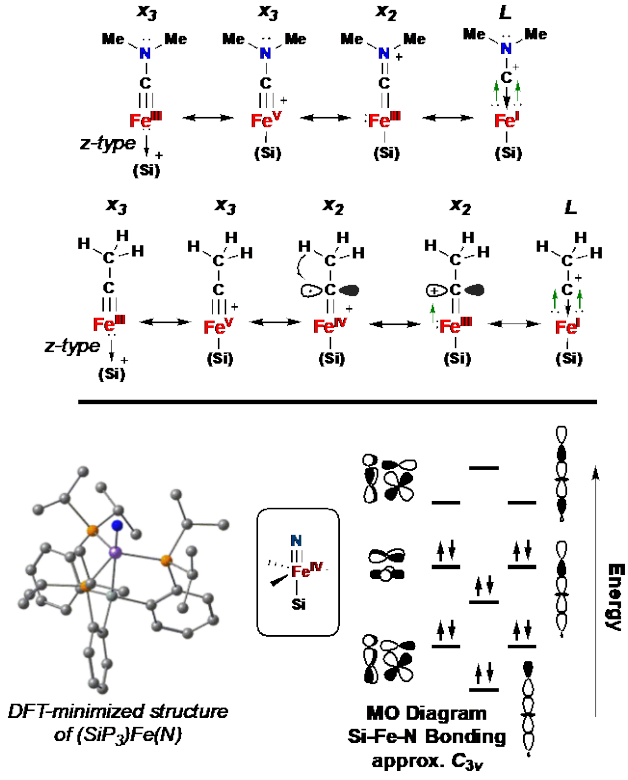

Figure 9. (top) Representative chemical depictions of the related amino- and alkylcarbynes $(SiP_3)Fe(CNMe_2)^+$ and $(SiP_3)Fe(CCH_3)^+$, along with formal iron valence assignments. The true relative state of oxidation at iron is presumed to vary little due to strong covalency. The primary bonding of the carbyne to iron is indicated as x_3, x_2, or L, with backbonds from iron into empty p-orbitals on carbon indicated by the green arrows. Note that a half-arrow is used to indicate hyperconjugation stabilization for the C-centered radical Fe(IV) form of $(SiP_3)Fe(CCH_3)^+$. (bottom) DFT-optimized structure of the hypothetical molecule $(SiP_3)Fe^{IV}(N)$, with a simplified MO diagram and lobal representations for the Si-Fe-N bonding in C_{3v} symmetry.

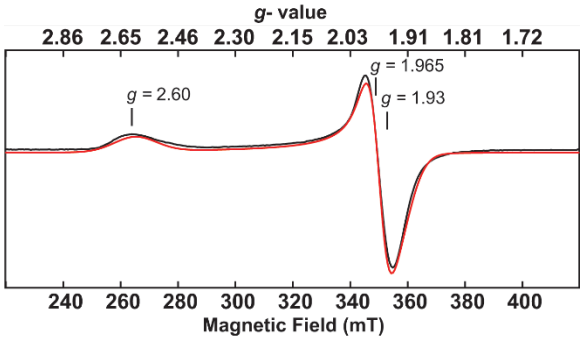

Figure 10. X-band CW-EPR spectrum of $[(SiP_3)FeCCH_3]OTf$ prepared in 7:1 2-MeTHF/MeCN. Acquisition parameters: temperature = 10 K; MW frequency = 9.637 GHz; MW power = 200 μW; modulation frequency = 100 kHz; modulation amplitude = 0.4 mT; conversion time = 82 ms.

To further probe the electronic structure of paramagnetic $[Fe{\equiv}CCH_3]^+$ **7** we undertook CW and pulse EPR studies. The doublet ground state of **7** can only be observed by EPR at very low temperatures due to fast electronic relaxation and line broadening at 77 K. At 10 K, an axial EPR spectrum exhibiting significant anisotropy between *g*-parallel at 2.61 and *g*-perpendicular at 1.96-1.93 is resolved (Figure 10), consistent with a largely iron-centered spin. Electron spin inversion recovery experiments show a strong temperature dependence for T_1 spin relaxation (Figure S41). This behavior is likely consistent with a low-lying, thermally populated doublet excited state or efficient electronic relaxation through coupling of low-energy vibrations (< 100 cm^{-1}) with the bath. If an Orbach mechanism of electronic relaxation from the excited state is assumed,[37] a small energy difference (Δ) between the ground state and first excited state as low as Δ = 24 cm^{-1} can be roughly calculated from the temperature dependence of T_1.[38]

EPR analysis of a paramagnetic carbyne/alkylidyne has previously been limited to a tungsten methylidyne cation $([(dmpe)_2(Cl)W^V{\equiv}CH]^+$; g_{iso} = 2.026; $|A(^{138}W)|$ = 221 MHz; $|A(^{31}P)|$ = 149 MHz; $|A(^{13}C)|$ = 34 MHz; dmpe = bis(dimethylphosphino)ethane) and to examples with the $(SiP_3)Fe$-system.[27c,12] Interestingly, $[(SiP_3)FeCNMe_2]^+$ and $[Fe{\equiv}CCH_3]^+$ **7** both exhibit nearly identical EPR signatures.[11] Löwdin spin population and spin density analysis of **7** by DFT (TPSS/def2-TZVP/D3ZERO) predicts the majority of unpaired spin on iron (0.99 e^-), with 0.07 e^- of opposite spin polarization on $C_α$ (Figure 8) (cf. $[(SiP_3)FeCNMe_2]^+$: 0.97 e^- on Fe, oppositely polarized to 0.03 e^- on $C_α$ and 0.01 e^- on $N_β$). This prediction is in agreement with the large anisotropy between *g*-parallel and *g*-perpendicular and the strong temperature dependence observed for T_1 (Figure S41).

This predicted spin delocalization compares very well with that for a terminal iron(V)-nitride reported by Smith and coworkers.[33] A follow-up study on this system[39] invoked a dynamic "pseudo Jahn-Teller" distortion for a C_3-symmetric iron center. Related electronic structure descriptions have been offered for ostensibly low-valent *S* = 1/2 $(SiP_3)Fe(H_2)$ and $TPBCo(H_2)$ complexes.[40] In Smith's iron(V)-nitride complex, vibronic coupling to a partially filled, degenerate $d(x^2-y^2)/d(xy)$ pair gives rise to significant *g*-anisotropy and mixing with the unfilled d(xz)/d(yz) pair – termed "e−e mixing" – yielding some spin delocalization onto the terminal nitride p-orbitals.[39] The electronic structure of $[Fe{\equiv}CCH_3]^+$ **7** can likely be understood by a similar model: a nearly degenerate *S* = 1/2 ground state leads to large *g*-anistropy and mixing of unoccupied d(xz)/d(yz) Fe-C $π^*$-bond orbitals with partially filled $d(xy)/d(x^2-y^2)$ orbitals delocalizes modest spin onto $C_α$ of the paramagnetic carbyne (Figure 8).[41]

Table 3. Hyperfine coupling constants in MHz determined for $[(SiP_3)FeCCH_3]^+$ and computed spin densities.

Nucleus	A_1	A_2	A_3	a_{iso}	Spin density
Fe					0.99
^{31}P	18	14	25	19.0	0.016 0.008 0.015
$^{13}C_α$	18	33	47	32.7	-0.067
$^{13}C_β$	5.8	5.0	4.0	4.9	-0.006
$^{1}H_3C$	8.6 2.3	12.5 6.3	8.6 6.3	9.9 5.0	-0.004 -0.001 -0.0002

As a direct probe of this hypothesis, pulse X-band HYSCORE and ENDOR spectroscopy of **7** was undertaken (Figures 11 and 12). From these complementary methods, comparison of data from (**$^{13}C_2$-7**) and its natural abundance isotopologue shows hyperfine couplings for the ^{13}C nuclei of $C_α$ and $C_β$ with the spin on iron. Simulation of the data gives an anisotropic hyperfine tensor for $^{13}C_α$ $|A(^{13}C)|$ = [18, 33, 47] MHz; a_{iso} = 32.7 MHz; *T* = 14.5 MHz) (Table 3), indicative of strong coupling to the $^{13}C_α$ nuclear spin. Coupling to $^{13}C_β$ is weaker and nearly isotropic ($|A(^{13}C)|$ = [5.8, 5.0, 4.0] MHz; a_{iso} = 4.9 MHz; *T* = 0.9 MHz). Following the analysis of Hoffman and coworkers,[39] the $^{13}C_α$ hyperfine coupling tensor can be decomposed into isotropic and anisotropic terms; the anisotropic component allows estimation of spin density of approximately 0.06 electrons at $C_α$ in the 2p(x) and 2p(y) orbitals, orthogonal to the *Fe*≡*C*-R bond vector. This estimate agrees well with the aforementioned Löwdin spin population analysis.

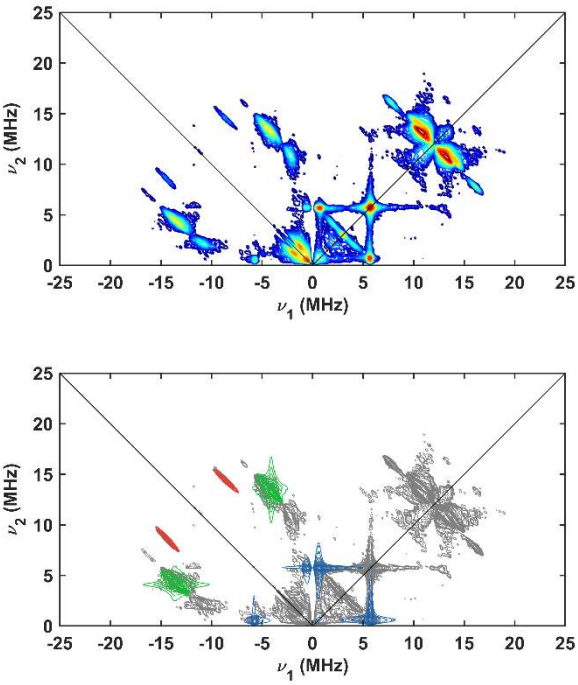

Figure 11. (top) X-band HYSCORE spectrum of $^{13}C_2$-[(SiP$_3$)FeCCH$_3$]OTf measured at 280 mT (g = 2.48) (Bottom) Monochromatic representation of the HYSCORE data with simulations of hyperfine couplings overlaid: (green) using simulations parameters in Table 3: (green) ^{31}P, (red) $^{13}C_\alpha$, (blue) $^{13}C_\beta$. Acquisition parameters: Acquisition parameters: temperature = 6.5 K; microwave frequency = 9.715 GHz; MW pulse length ($\pi/2$, π) = 8 ns, 16 ns; τ = 168 ns, $t_1 = t_2$ = 100 ns; $\Delta t_1 = \Delta t_2$ = 16 ns; shot repetition time (srt) = 1 ms).

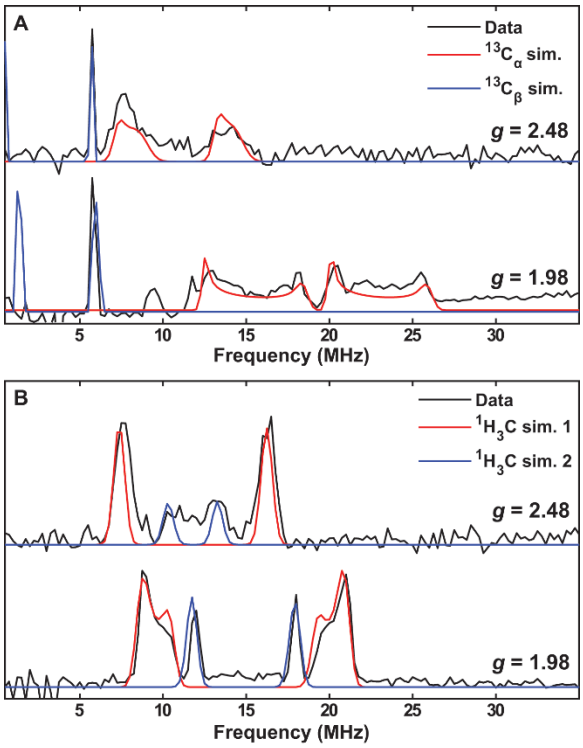

Figure 12. (A) (black) X-band ^{13}C-^{12}C difference ENDOR spectra of (**$^{13}C_2$-7**) and (**$^{12}C_2$-7**); (red) $^{13}C_\alpha$ simulated fit; (blue) $^{13}C_\beta$ simulated fit. (B) (black) X-band ^{1}H-^{2}H difference ENDOR spectra of (**^1H_3C-7**) and (**^2H_3C-7**); (red) ^1H_3C simulated fit 1; (blue) ^1H_3C simulated fit 2. Acquisition parameters: temperature = 6.5 K; MW frequency = 9.715 GHz; MW pulse length ($\pi/2$, π) = 40 ns, 80 ns; τ = 190 ns; RF pulse length = 15 µs; T_{RF} = 2 µs; shot repetition time = 5 ms.

Interestingly, despite weak coupling to C_β, proton hyperfine coupling to the -CH$_3$ substituent of [Fe≡CCH$_3$]$^+$ **7** is detected by both ENDOR and HYSCORE. Comparison of **^{2}H-7** with its natural abundance isotopologue and simulation of the ENDOR difference spectrum (Figure 12) provides two hyperfine tensors for $^1H_1(CH_3)$ ($|A(^1H)|$ = [8.6, 12.5, 8.6] MHz; a_{iso} = 9.9 MHz; T = 1.3 MHz) and $^1H_2(CH_3)$ ($|A(^1H)|$ = [2.3, 6.3, 6.3] MHz; a_{iso} = 5.0 MHz; T = 1.3 MHz). Importantly, the isotropic coupling components for the carbyne -*CH$_3$* substituent to the unpaired spin are correlated with a "hyperconjugation" interaction between the methyl H-atoms and the spin active Fe and C_α orbitals.[42,43,44]

A hyperconjugation effect indicates, to some extent, delocalization of spin/hole or cationic character on Fe≡C_α to the hydrogen s-orbitals on the terminal methyl (see Figure 9 for this and other chemical depictions). This exaggerated resonance description is thus juxtaposed with the electronic structures typically invoked in heteroatom-substituted carbyne complexes, like our previously reported (SiP$_3$)FeCOSiMe$_3$, (DPB)Fe(COSiMe$_3$)$_2$, [(SiP$_3$)FeCNMe$_2$]$^{0/+}$, and [(SiP$_3$)FeCNH$_2$]$^+$ [20–23]. In each of these cases, the Fe-C and C-O/N bonding is qualified by the free "lone pair" on the distal atom, capable of delocalizing bonding across the Fe-C-O/N unit and decreasing the formal valency at iron. The CNR$_2$ moiety of the amino carbynes are even planar ($\Sigma\angle \approx 360°$), consistent with conjugation between nitrogen and the Fe-C π-bond. However, hyperconjugation and delocalization in [(SiP$_3$)FeCCH$_3$]$^+$ should be appreciated as a subtle effect, as the spectroscopic data and DFT calculations determine a majority of unpaired spin to be located on iron (Fe: +0.99 e$^-$ vs. C_α: -0.07 e$^-$). Furthermore, the strong similarity between the EPR data for [(SiP$_3$)FeCNMe$_2$]$^+$ and [(SiP$_3$)FeCCH$_3$]$^+$, the comparably modest calculated spin density across the amino carbyne (Fe: +0.97 e$^-$ vs C_α: -0.03 e$^-$ and N_β: -0.01 e$^-$), and the close congruence between the Mössbauer parameters for all of the (SiP$_3$)Fe carbynes, both alkyl- and heteroatom-substituted, suggests that a "Fischer-like" resonance description (the L-type carbyne donor resonance forms in Figure 9) may in fact be of limited importance to the structural and electronic stabilities of this series of Fe≡C triply bonded species.

The latter point speaks to the potential relevance of other hypothetical iron-ligand multiply-bonded species in the (SiP$_3$)Fe platform, namely terminal Fe≡C(H) carbide/methylidyne or Fe≡N nitride complexes (Figure 9, bottom), the latter possibly arising during the limited nitrogen reduction catalysis mediated by (SiP$_3$)FeN$_2$;[45] the former have yet to be directly evidenced from cleavage of CO, CN$^-$, or C_2H_2 at iron. We have extensively explored the reactivity and thermochemistry of the early stages of reductive protonation on FeN$_2$ compounds. In the trisphosphine-borane TPBFeN$_2$, the N-N bond is cleaved to yield NH$_3$ and a spectroscopically characterized [(TPB)Fe^{IV}≡N]$^+$ nitride cation.[3] Observation of an iron-N_2H_4 hydrazine cation[46] derived from (SiP$_3$)FeN$_2$ questions the accessibility of any (SiP$_3$)Fe≡N species through functionalization of dinitrogen. However, the stable bonding in the [(SiP$_3$)FeCCH$_3$]$^{+/0}$ complexes, and the aforementioned implication for the electronic structures of the heteroatom-substituted relatives, support the potential viability of high-valent, multiply-bonded Fe≡C or Fe≡N intermediates in the chemistry of this system, and structurally related synthetic or biological iron sites.

CONCLUSION

To close, we have described the activation of acetylene gas at a mononuclear iron site, along with reductive protonation reactions that converge at stable and structurally unusual Fe(IV) and Fe(V) alkylcarbyne complexes. X-ray crystallography, pulse X-band EPR, and other spectroscopies have allowed us to characterize the first Fe(I) and Fe(II) adducts of acetylene, and to discriminate their side-on binding forms from alternative structural isomers (e.g., $Fe{=}CCH_2$). Characterization of their electronic structures, through Mössbauer, DFT, and pulse EPR experiments, reveal strong covalency in the Fe≡C triple bonds of the carbyne species and moderate spin delocalization in the cationic $S = 1/2$ congeners. Congruence between the structural, spectroscopic, and computed parameters of the heteroatom-substituted iron carbynes with those of the newly explored alkylcarbynes described here establishes the viability of a highly covalent Fe-to-C triple bond in trigonal pyramidal symmetry without a requirement for heteroatom resonance stabilization. More generally, the complexes and spectroscopic signatures reported here may guide the ongoing investigation of reactive nitrogenase intermediates with non-native substrates, particularly acetylenic adduct species, or possible carbyne intermediates of Fischer-Tropsch type C-C couplings with C_1 substrates.

ASSOCIATED CONTENT

Supporting Information

The Supporting Information is available free of charge on the ACS Publications website at DOI:

Procedures and characterization data (PDF)
X-ray Data (CIF)
Computational models (inp)

AUTHOR INFORMATION

Corresponding Authors

jpeters@caltech.edu

Notes

The authors declare no competing financial interest.

ACKNOWLEDGMENT

This work was supported by the National Institutes of Health (General Medical Sciences, grant GM070757). C.C. acknowledges the NIH Ruth L. Kirschstein National Service Fellowship for financial support. Additional support has been provided by the Caltech EPR Facility, supported via NSF-1531940, and the Dow Next Generation Educator Fund. We also acknowledge the Beckman Institute for use of the its X-ray facility and thank Larry M. Henling and Dr. David G. VanderVelde for technical assistance with X-ray and NMR experiments, respectively.

References

[1] For representative reviews and several lead references, see: (a) Berry, J. F. Terminal Imido and Nitrido Complexes of the Late Transition Metals. *Comm. Inorg. Chem.* **2009**, *30*, 28-66. (b) Saouma, C. A.; Peters, J. C. M≡E and M=E Complexes of Iron and Cobalt that Emphasize Three-Fold Symmetry (E = O, N, NR). *Coord. Chem. Rev.* **2011**, *255*, 920-937. (c) Mondal, B.; Roy, L.; Neese, F.; Ye, S. F. High-Valent Iron-Oxo and -Nitrido Complexes: Bonding and Reactivity. *Isr. J. Chem.* **2016**, *56*, 763-772. (d) Wagner, W. D.; Nakamoto, K. Formation of Nitridoiron(V) Porphyrins Detected by Resonance Raman Spectroscopy. *J. Am. Chem. Soc.* **1988,** *110*, 4044-4045; (e) Meyer, K.; Bill, E.; Mienert, B.; Weyhermüller, T.; Wieghardt, K. Photolysis of cis- and trans-$[Fe^{III}(cyclam)(N_3)_2]^+$ Complexes: Spectroscopic Characterization of a Nitridoiron(V) Species. *J. Am. Chem. Soc.* **1999,** *121*, 4859-4876; (f) Berry, J. F.; Bill, E.; Bothe, E.; George, S. D.; Mienert, B.; Neese, F.; Wieghardt, K. An Octahedral Coordination Complex of Iron(VI). *Science* **2006,** *312*, 1937-1941; (g) Aldrich, K. E.; Billow, B. S.; Holmes, D.; Bemowski, R. D.; Odom, A. L. Weakly Coordinating yet Ion Paired: Anion Effects on an Internal Rearrangement. *Organometallics* **2017**, *36*, 1227–1237; (h) Martinez, J. L.; Lin, H.-J.; Lee, W.-T.; Pink, M.; Chen, C.-H.; Gao, X.; Dickie, D. A.; Smith, J. M. Cyanide Ligand Assembly by Carbon Atom Transfer to an Iron Nitride. *J. Am. Chem. Soc.* **2017**, *139*, 14037–14040; (i) Bucinsky, L.; Breza, M.; Lee, W.-T.; Hickey, A. K.; Dickie, D. A.; Nieto, I.; DeGayner, J. A.; Harris, T. D.; Meyer, K.; Krzystek, J.; Ozarowski, A.; Nehrkorn, J.; Schnegg, A.; Holldack, K.; Herber, R. H.; Telser, J.; Smith, J. M. Spectroscopic and Computational Studies of Spin States of Iron(IV) Nitrido and Imido Complexes. *Inorg. Chem.* **2017**, *56*, 4751–4768.

[2] (a) Betley, T. A.; Peters, J. C. A Tetrahedrally Coordinated $L_3Fe{-}N_x$ Platform that Accommodates Terminal Nitride ($Fe^{IV}{\equiv}N$) and Dinitrogen ($Fe^{I}{-}N_2{-}Fe^{I}$) Ligands. *J. Am. Chem. Soc.* **2004,** *126*, 6252-6254. (b) Hendrich, M. P.; Gunderson, W.; Behan, R. K.; Green, M. T.; Mehn, M. P.; Betley, T. A.; Lu, C. C.; Peters, J. C. On the Feasibility of N_2 Fixation via a Single-Site Fe^{I}/Fe^{IV} Cycle: Spectroscopic Studies of $Fe^{I}(N_2)Fe^{I}$, $Fe^{IV}N$, and Related Species. *PNAS* **2006**, *103*, 17107–17112.

[3] Thompson, N. B.; Green, M. T.; Peters, J. C. Nitrogen Fixation via a Terminal Fe(IV) Nitride. *J. Am. Chem. Soc.* **2017**, *139*, 15312–15315.

[4] (a) Lee, C. C.; Hu, Y.; Ribbe, M. W. Catalytic Reduction of CN−, CO, and CO_2 by Nitrogenase Cofactors in Lanthanide-Driven Reactions. *Angew. Chem. Int. Ed.* **2015**, *54*, 1219–1222. (b) Lee, C. C.; Hu, Y.; Ribbe, M. W. Vanadium Nitrogenase Reduces CO. *Science* **2010**, *329*, 642–642. (c) Hu, Y.; Lee, C. C.; Ribbe, M. W. Extending the Carbon Chain: Hydrocarbon Formation Catalyzed by Vanadium/Molybdenum Nitrogenases. *Science* **2011**, *333*, 753–755. (d) Yang, Z.-Y.; Dean, D. R.; Seefeldt, L. C. Molybdenum Nitrogenase Catalyzes the Reduction and Coupling of CO to Form Hydrocarbons. *J. Biol. Chem.* **2011**, *286*, 19417–19421. (e) Spatzal, T.; Perez, K. A.; Einsle, O.; Howard, J. B.; Rees, D. C. Ligand Binding to the FeMo-Cofactor: Structures of CO-Bound and Reactivated Nitrogenase. *Science* **2014**, *345*, 1620-1623.

[5] Burgess, B. K.; Lowe, D. J. Mechanism of Molybdenum Nitrogenase. *Chem. Rev.* **1996**, *96*, 2983–3012.

[6] Dilworth, M. J.; Fisher, K.; Kim, C.-H.; Newton, W. E. Effects on Substrate Reduction of Substitution of Histidine-195 by Glutamine in the α-Subunit of the MoFe Protein of Azotobacter Vinelandii Nitrogenase. *Biochemistry* **1998**, *37*, 17495–17505.

[7] Kim, C.-H.; Newton, W. E.; Dean, D. R. Role of the MoFe Protein .Alpha.-Subunit Histidine-195 Residue in FeMo-Cofactor Binding and Nitrogenase Catalysis. *Biochemistry* **1995**, *34*, 2798–2808.

[8] Fischer, E. O.; Schneider, J.; Neugebauer, D. $[(CO)_3PPh_3FeCNiPr_2]^+$, a Novel Stable Carbyneiron Complex Cation. *Angew. Chem. Int. Ed. Engl.* **1984**, *23*, 820–821.

[9] Lee, Y.; Peters, J. C. Silylation of Iron-Bound Carbon Monoxide Affords a Terminal Fe Carbyne. *J. Am. Chem. Soc.* **2011**, *133*, 4438–4446.

[10] Suess, D. L. M.; Peters, J. C. A CO-Derived Iron Dicarbyne That Releases Olefin upon Hydrogenation. *J. Am. Chem. Soc.* **2013**, *135*, 12580–12583.

[11] Rittle, J.; Peters, J. C. Proton-Coupled Reduction of an Iron Cyanide Complex to Methane and Ammonia. *Angew. Chem. Int. Ed.* **2016**, *55*, 12262–12265.

[12] Rittle, J.; Peters, J. C. N–H Bond Dissociation Enthalpies and Facile H Atom Transfers for Early Intermediates of Fe–N_2 and Fe–CN Reductions. *J. Am. Chem. Soc.* **2017**, *139*, 3161–3170.

[13] Benton, P. M. C.; Laryukhin, M.; Mayer, S. M.; Hoffman, B. M.; Dean, D. R.; Seefeldt, L. C. Localization of a Substrate Binding Site on the FeMo-Cofactor in Nitrogenase: Trapping Propargyl Alcohol with an α-70-Substituted MoFe Protein. *Biochemistry* **2003**, *42*, 9102–9109.

[14] For structurally characterized examples of Fe-CCH complexes see: (a) Le Narvor, N.; Toupet, L.; Lapinte, C. Elemental Carbon Chain Bridging Two Iron Centers: Syntheses and Spectroscopic Properties of $[Cp^*(dppe)Fe{-}C_4{-}FeCp^*(dppe)]^{n+}{\bullet}n[PF_6]^-$. X-Ray Crystal Structure of the Mixed Valence Complex (n = 1). *J. Am. Chem. Soc.* **1995**, *117*, 7129–7138. (b) Dahlenburg, L.; Weiβ, A.; Bock, M.; Zahl, A. Ethinyl- Und Butadiinylkomplexe Des Eisens Und Rutheniums Mitterminalen Hauptgruppenelement-Substituenten, Cp^* $Fe(Ph_2PCH(X)CH_2PPh_2)$ C ≡ CY (X = H, PPh_2; Y = H, PPh_2, $P^{(+)}Ph_2Me$) Und $Ru(Ph_2PCH_2PPh_2)_2(X)$ C ≡ CC ≡ $CSiMe_3$ (X = Cl, C ≡ CC ≡ $CSiMe_3$). *J. Organomet. Chem.* **1997**, *541*, 465–471. (c) Akita, M.; Terada, M.; Oyama, S.; Morooka, Y. Preparation, Structure, and Divergent Fluxional Behavior of Cationic Dinuclear Iron Acetylides $[Fp^*_2(C{\equiv}CR)]BF_4$ (R = H, Ph). *Organometallics* **1990**, *9*, 816–825.

[15] Lee, Y.; Mankad, N. P.; Peters, J. C. Triggering N_2 Uptake via Redox-Induced Expulsion of Coordinated NH_3 and N_2 Silylation at Trigonal Bipyramidal Iron. *Nat. Chem.* **2010**, *2*, 558–565.

[16] Bennett, M. A. Olefin and Acetylene Complexes of Transition Metals. *Chem. Rev.* **1962**, *62*, 611–652.

[17] For structurally characterized examples of mononuclear C_2H_2 complexes of Cr, Ni, and Cu, see: (a) Alt, H. G.; Han, J. S.; Rogers, R. D.; Thewalt, U. Acetylenkomplexe des Wolframs. Molekülstrukturen von $(\eta^5\text{-}C_5H_4CMe_2C_{13}H_9)W(CO)(HC_2Ph)Me$, $(\eta^5{:}\ \eta^1\text{-}C_5H_4CMe_2C_{13}H_8)W(CO)(C_2Ph_2)$ und $(\eta^5\text{-}C_5H_5)Cr(CO)(C_2H_2)NO$; ein Vergleich von alkinischen Vier- und Zweielektronenliganden. *J. Organomet. Chem.* **1993**, *459*, 209–217. (b) Munakata, M.; Kitagawa, S.; Kawada, I.; Maekawa, M.; Shimono, H. Synthesis, Formation Constants and Structures of Ternary Copper(I) Complexes with 1,10-Phenanthroline and Alkynes. *J. Chem. Soc., Dalton Trans.* **1992**, *14*, 2225–2230. (c) Pörschke, K. R.; Tsay, Y.-H.; Krüger, C. Ethynebis(Triphenylphosphane)Nickel(0). *Angew. Chem. Int. Ed.* **1985**, *24*, 323–324. (d) Thompson, J. S.; Whitney, J. F. Copper(I) Complexes with Unsaturated Small Molecules. Preparation and Structural Characterization of Copper(I)-Di-2-Pyridylamine Complexes with Olefins, Acetylene, and Carbon Monoxide. *Inorg. Chem.* **1984**, *23*, 2813–2819. (e) Thompson, J. S.; Whitney,

J. F. Preparation and Structural Characterization of Acetylene(2,2'-Dipyridylamine)Copper(I) Tetrafluoroborate. *J. Am. Chem. Soc.* **1983**, *105*, 5488–5490.

[18] Overend, J. The Equilibrium Bond Lengths in Acetylene and HCN. *Trans. Faraday Soc.* **1960**, *56*, 310–314.

[19] Buscagan, T. M.; Oyala, P. H.; Peters, J. C. N_2-to-NH_3 Conversion by a Triphos–Iron Catalyst and Enhanced Turnover under Photolysis. *Angew. Chem. Int. Ed.* **2017**, *56*, 6921–6926.

[20] Gu, N. X.; Oyala, P. H.; Peters, J. C. An S = 1/2 Iron Complex Featuring N_2, Thiolate, and Hydride Ligands: Reductive Elimination of H_2 and Relevant Thermochemical Fe–H Parameters. *J. Am. Chem. Soc.* **2018**, *140*, 6374–6382.

[21] (a) Stoian, S. A.; Yu, Y.; Smith, J. M.; Holland, P. L.; Bominaar, E. L.; Münck, E. Mössbauer, Electron Paramagnetic Resonance, and Crystallographic Characterization of a High-Spin Fe(I) Diketiminate Complex with Orbital Degeneracy. *Inorg. Chem.* **2005**, *44*, 4915–4922. (b) Yu, Y.; Smith, J. M.; Flaschenriem, C. J.; Holland, P. L. Binding Affinity of Alkynes and Alkenes to Low-Coordinate Iron. *Inorg. Chem.* **2006**, *45*, 5742–5751. (c) Horitani, M.; Grubel, K.; McWilliams, S. F.; Stubbert, B. D.; Mercado, B. Q.; Yu, Y.; Gurubasavaraj, P. M.; Lees, N. S.; Holland, P. L.; Hoffman, B. M. ENDOR Characterization of an Iron–Alkene Complex Provides Insight into a Corresponding Organometallic Intermediate of Nitrogenase. *Chem. Sci.* **2017**, *8*, 5941–5948.

[22] (a) Bianchini, Claudio.; Peruzzini, Maurizio.; Vacca, Alberto.; Zanobini, Fabrizio. Metal-Hydride Alkynyl→Metal-Vinylidene Rearrangements Occurring in Both Solid State and Solution. Role of the 1-Alkyne Substituent in Determining the Relative Stability of π-Alkyne, Hydride Alkynyl, and Vinylidene Forms at Cobalt. *Organometallics* **1991**, *10*, 3697–3707. (b) Bianchini, Claudio.; Masi, Dante.; Meli, Andrea.; Peruzzini, Maurizio.; Ramirez, J. A.; Vacca, Alberto.; Zanobini, Fabrizio. Activation of 1-Alkynes at 16-Electron Rhodium Fragments. Some Examples of Thermodynamically Favored Rearrangements [M(π-HC≡CR)] → [M(H)(C≡CR)]. *Organometallics* **1989**, *8*, 2179–2189. (c) Gauss, C.; Veghini, D.; Orama, O.; Berke, H. The Reactions of Dicarbonylbis(Phosphorus Donor) Iron Fragments with Tertiary Propargyl Alcohols. *J. Organomet. Chem.* **1997**, *541*, 19–38. (d) Pombeiro, A. J. L.; Hills, A.; Hughes, D. L.; Richards, R. L. Synthesis and Crystal Structure of $[MoH_3(C{\equiv}CBu^t)(Ph_2PCH_2CH_2PPh_2)_2]$, a Trihydrido-Alkynyl Complex. *J. Organomet. Chem.* **1990**, *398*, C15–C18. (e) Basallote, M. G.; Hughes, D. L.; Jiménez-Tenorio, M.; Leigh, G. J.; Vizcaíno, M. C. P.; Jiménez, P. V. Chemistry of Cobalt Complexes with 1,2-Bis-(Diethylphosphino)Ethane: Hydrides, Carbon Disulfide Complexes, and C–H Cleavage in Activated Alk-1-Ynes. Crystal Structure of $[CoH(C{\equiv}CCO_2Et)(Et_2PCH_2CH_2PEt_2)_2][BPh_4]$. *J. Chem. Soc., Dalton Trans.* **1993**, *0*, 1841–1847. (f) Ittel, S. D.; Tolman, C. A.; English, A. D.; Jesson, J. P. The Chemistry of 2-Naphthyl Bis[Bis(Dimethylphosphino)Ethane] Hydride Complexes of Iron, Ruthenium, and Osmium. 2. Cleavage of sp and sp^3 Carbon-Hydrogen, Carbon-Oxygen, and Carbon-Halogen Bonds. Coupling of Carbon Dioxide and Acetonitrile. *J. Am. Chem. Soc.* **1978**, *100*, 7577–7585. (g) Field, L. D.; George, A. V.; Malouf, E. Y.; Hambley, T. W.; Turner, P. A Reductive Rearrangement of Iron Acetylide Hydridecomplexes. *Chem. Commun.* **1997**, *0*, 133–134.

[23] Fong, H.; Moret, M.-E.; Lee, Y.; Peters, J. C. Heterolytic H_2 Cleavage and Catalytic Hydrogenation by an Iron Metallaboratrane. *Organometallics* **2013**, *32*, 3053–3062.

[24] Bruce, M. I. Organometallic Chemistry of Vinylidene and Related Unsaturated Carbenes. *Chem. Rev.* **1991**, *91*, 197–257.

[25] (a) Lomprey, J. R.; Selegue, J. P. Structural Characterization of Alkyne and Vinylidene Isomers of $[Ru(C_2H_2)(PMe_2Ph)_2(Cp)][BF_4]$. *J. Am. Chem. Soc.* **1992**, *114*, 5518–5523. (b) Consiglio, G.; Bangerter, F.; Darpin, C.; Morandini, F.; Lucchini, V. Diastereomeric Equilibria and Barrier of Rotation in Cationic Iron Diphosphine Alkylidenecarbene (Vinylidene) Complexes. *Organometallics* **1984**, *3*, 1446–1448. (c) Bullock, R. M. Rearrangement of a Metal (H_2-Alkyne) Complex to a Metal Vinylidene and Subsequent Reaction of the Metal Vinylidene to Regenerate the Alkyne. *J. Chem. Soc., Chem. Commun.* **1989**, *0*, 165–167. (d) Fryzuk, M. D.; Huang, L.; McManus, N. T.; Paglia, P.; Rettig, S. J.; White, G. S. Synthesis and Reactivity of the Iridium Vinylidene $Ir{:}C{=}CH_2[N(SiMe_2CH_2PPh_2)_2]$. Formation of Carbon-Carbon Bonds via Migratory Insertion of a Vinylidene Unit. *Organometallics* **1992**, *11*, 2979–2990. (e) Birdwhistell, K. R.; Burgmayer, S. J. N.; Templeton, J. L. Tungsten Vinylidenes and Carbynes from Terminal Alkyne Reagents. *J. Am. Chem. Soc.* **1983**, *105*, 7789–7790.

[26] Gauss, C.; Veghini, D.; Berke, H. Acetylene/Vinylidene Rearrangements of $Fe(CO)_2L_2$(silylacetylene) Complexes (L = Phosphorus Donor). *Chem. Ber.* **1997**, *130*, 183–194.

[27] (a) Felixberger, J. K.; Kiprof, P.; Herdtweck, E.; Herrmann, W. A.; Jakobi, R.; Gütlich, P. Alkyl and Alkylidyne Complexes of Rhenium. *Angew. Chem. Int. Ed. Engl.* **1989**, *28*, 334–337. (b) N.D.A. Lemos, M. A.; Pombeiro, A. J. L.; Hughes, D. L.; Richards, R. L. Synthesis and X-Ray Crystal Structure of Trans-$[MoF(\equiv CCH_2tBu)(Ph_2PCH_2CH_2PPh_2)_2][BF_4]$, a Paramagnetic Alkylidynefluorocomplex. *J. Organomet. Chem.* **1992**, *434*, C6–C9. (c) van der Eide, E. F.; Piers, W. E.; Parvez, M.; McDonald, R. Synthesis and Characterization of Cationic Tungsten(V) Methylidynes. *Inorg. Chem.* **2007**, *46*, 14–21. (d) Leep, C. J.; Kingsbury, K. B.; McElwee-White, Lisa. Photooxidation of $(\eta\text{-}C_5H_5)[P(OMe)_3]_2Mo{\equiv}CPh$ in $CHCl_3$. Intermediacy of a 17-Electron Cationic Metal Carbyne. *J. Am. Chem. Soc.* **1988**, *110*, 7535–7536.

[28] Paramagnetic carbenes are well known. See, for example, Dzik, W. I.; Zhang, X. P.; de Bruin, B. Redox Noninnocence of Carbene Ligands: Carbene Radicals in (Catalytic) C−C Bond Formation. *Inorg. Chem.* **2011**, *50*, 9896–9903 and references therein.

[29] It appears that $[FeCCH]^+$ can be generated via oxidation of **3** by $[Cp_2Fe][BArF_{24}]$; preliminary characterization data for $[(SiP_3)FeCCH]^+$ is available in the Supporting Information.

[30] Clark, D. N.; Schrock, R. R. Multiple Metal-Carbon Bonds. 12. Tungsten and Molybdenum Neopentylidyne and Some Tungsten Neopentylidene Complexes. *J. Am. Chem. Soc.* **1978**, *100*, 6774–6776.
[31] Köhler, F. H.; Kalder, H. J.; Fischer, E. O. Die Metall-Kohlenstoff-Bindung in Carben- Und Carbin-Komplexen. Aussagen Der $^{183}W\equiv^{13}C$-Kopplungen. *J. of Organom. Chem.* **1976**, *113*, 11–22.
[32] Gütlich, P.; Bill, E.; Trautwein, A. *Mössbauer Spectroscopy and Transition Metal Chemistry: Fundamentals and Application*; Springer: Berlin ; Heidelberg, 2011.
[33] Scepaniak, J. J.; Vogel, C. S.; Khusniyarov, M. M.; Heinemann, F. W.; Meyer, K.; Smith, J. M. Synthesis, Structure, and Reactivity of an Iron(V) Nitride. *Science* **2011**, *331*, 1049–1052.
[34] Oliveira, F. T. de; Chanda, A.; Banerjee, D.; Shan, X.; Mondal, S.; Que, L.; Bominaar, E. L.; Münck, E.; Collins, T. J. Chemical and Spectroscopic Evidence for an Fe^{V}-Oxo Complex. *Science* **2007**, *315*, 835–838.
[35] Nance, P. J.; Thompson, N. B.; Oyala, P. H.; Peters, J. C. Zerovalent Rhodium and Iridium Silatranes Featuring Two-Center, Three-Electron Polar σ Bonds. *Angew. Chem. Int. Ed.* **2019**, *58*, 6220–6224.
[36] Takaoka, A.; Moret, M.-E.; Peters, J. C. A Ru(I) Metalloradical That Catalyzes Nitrene Coupling to Azoarenes from Arylazides. *J. Am. Chem. Soc.* **2012**, *134*, 6695–6706.
[37] (a) Orbach, R. Spin-lattice Relaxation in Rare-Earth Salts. *Proc. R. Soc. Ser. A.* **1961**, *264*, 458-484. (b) Orbach, R. Spin-lattice Relaxation in Rare-Earth Salts: Field Dependence of the Two Phonon Processes. *Proc. R. Soc. Ser. A.* **1961**, *264*, 485-495.
[38] (a) Lorigan, G. A.; Britt, R. D. Electron Spin-Lattice Relaxation Studies of Different Forms of the S2 State Multiline EPR Signal of the Photosystem II Oxygen-Evolving Complex. *Photosynth. Res.* **2000**, *66*, 189–198. (b) Su, J.-H.; Cox, N.; Ames, W.; Pantazis, D. A.; Rapatskiy, L.; Lohmiller, T.; Kulik, L. V.; Dorlet, P.; Rutherford, A. W.; Neese, F.; Boussac, A.; Lubitz, W.; Messinger, J. The Electronic Structures of the S2 States of the Oxygen-Evolving Complexes of Photosystem II in Plants and Cyanobacteria in the Presence and Absence of Methanol. *Biochim. Biophys. Acta, Bioenerg.* **2011**, *1807*, 829–840.
[39] Cutsail III, G. E.; Stein, B. W.; Subedi, D.; Smith, J. M.; Kirk, M. L.; Hoffman, B. M. EPR, ENDOR, and Electronic Structure Studies of the Jahn–Teller Distortion in an Fe^{V} Nitride. *J. Am. Chem. Soc.* **2014**, *136*, 12323–12336.
[40] (a) Gunderson, W. A.; Suess, D. L. M.; Fong, H.; Wang, X.; Hoffmann, C. M.; Cutsail III, G. E.; Peters, J. C.; Hoffman, B. M. Free H_2 Rotation vs Jahn–Teller Constraints in the Nonclassical Trigonal (TPB)Co–H_2 Complex. *J. Am. Chem. Soc.* **2014**, *136*, 14998–15009. (b) Lee, Y.; Kinney, R. A.; Hoffman, B. M.; Peters, J. C. A Nonclassical Dihydrogen Adduct of S = 1/2 Fe(I). *J. Am. Chem. Soc.* **2011**, *133*, 16366–16369.
[41] We also note that a distortion in $[Fe\equiv CCH_3]^+$ **7** is reflected in the bonding metrics of the P_3Fe plane, while the Si-Fe-C vector remains approximately linear; in the aforementioned Fe(V)-nitride complex, the rigid tris(carbene) ligand cannot undergo such a distortion and instead manifests a nonlinear B-Fe-N vector. For related discussions of Mn systems, see: (a) Kropp, H.; King, A. E.; Khusniyarov, M. M.; Heinemann, F. W.; Lancaster, K. M.; DeBeer, S.; Bill, E.; Meyer, K. Manganese Nitride Complexes in Oxidation States III, IV, and V: Synthesis and Electronic Structure. *J. Am. Chem. Soc.* **2012**, *134*, 15538–15544; (b) Ding, M.; Cutsail, G. E., III; Aravena, D.; Amoza, M.; Rouzières, M.; Dechambenoit, P.; Losovyj, Y.; Pink, M.; Ruiz, E.; Clérac, R.; Smith, J. M. A Low Spin Manganese(IV) Nitride Single Molecule Magnet. *Chem. Sci.* **2016**, *7*, 6132–6140.
[42] McConnell, H. M. Electron Densities in Semiquinones by Paramagnetic Resonance. *J. Chem. Phys.* **1956**, *24*, 632–632.
[43] Heller, C.; McConnell, H. M. Radiation Damage in Organic Crystals. II. Electron Spin Resonance of $(CO_2H)CH_2CH(CO_2H)$ in β-Succinic Acid. *J. Chem. Phys.* **1960**, *32*, 1535–1539.
[44] A through-space mechanism of spin delocalization is reflected by the anisotropic coupling components.
[45] Del Castillo, T. J.; Thompson, N. B.; Peters, J. C. A Synthetic Single-Site Fe Nitrogenase: Higher Turnover, Freeze-Quench ^{57}Fe Mössbauer Data, and a Hydride Resting State. *J. Am. Chem. Soc.* **2016**, *138*, 5341–5350.
[46] Rittle, J.; Peters, J. C. An Fe-N_2 Complex that Generates Hydrazine and Ammonia via $Fe{=}NNH_2$: Demonstrating a Hybrid Distal to Alternating Pathway for N_2 Reduction. *J. Am. Chem. Soc.* **2016**, *138*, 4243–4248.

TOC Graphic: